

Accepted Manuscript



Mutations in Plasmalemma Vesicle Associated Protein (PLVAP) Result in Sieving Protein Losing Enteropathy Characterized by Hypoproteinemia, Hypoalbuminemia, and Hypertriglyceridemia

Abdul Elkadri, Cornelia Thoeni, Sophie J. Deharvengt, Ryan Murchie, Conghui Guo, James D. Stavropoulos, Christian R. Marshall, Paul Wales, Robert Bandsma, Ernest Cutz, Chaim M. Roifman, David Chitayat, Yaron Avitzur, Radu V. Stan, Aleixo M. Muise

PII: S2352-345X(15)00095-8
DOI: [10.1016/j.jcmgh.2015.05.001](https://doi.org/10.1016/j.jcmgh.2015.05.001)
Reference: JCMGH 39

To appear in: *Cellular and Molecular Gastroenterology and Hepatology*
Accepted Date: 4 May 2015

Please cite this article as: Elkadri A, Thoeni C, Deharvengt SJ, Murchie R, Guo C, Stavropoulos JD, Marshall CR, Wales P, Bandsma R, Cutz E, Roifman CM, Chitayat D, Avitzur Y, Stan RV, Muise AM, Mutations in Plasmalemma Vesicle Associated Protein (PLVAP) Result in Sieving Protein Losing Enteropathy Characterized by Hypoproteinemia, Hypoalbuminemia, and Hypertriglyceridemia, *Cellular and Molecular Gastroenterology and Hepatology* (2015), doi: 10.1016/j.jcmgh.2015.05.001.

This is a PDF file of an unedited manuscript that has been accepted for publication. As a service to our customers we are providing this early version of the manuscript. The manuscript will undergo copyediting, typesetting, and review of the resulting proof before it is published in its final form. Please note that during the production process errors may be discovered which could affect the content, and all legal disclaimers that apply to the journal pertain.

All studies published in Cellular and Molecular Gastroenterology and Hepatology are embargoed until 3PM ET of the day they are published as corrected proofs on-line. Studies cannot be publicized as accepted manuscripts or uncorrected proofs.

Mutations in Plasmalemma Vesicle Associated Protein (PLVAP) Result in Sieving Protein Losing Enteropathy Characterized by Hypoproteinemia, Hypoalbuminemia, and Hypertriglyceridemia

Abdul Elkadri^{1,2,3,#,§}, Cornelia Thoeni^{1,2,§,#}, Sophie J Deharvengt^{4#}, Ryan Murchie^{1,2,§}, Conghui Guo^{2,§}, James D Stavropoulos⁵, Christian R Marshall⁵, Paul Wales⁶, Robert Bandsma², Ernest Cutz⁷, Chaim M Roifman⁸, David Chitayat⁹, Yaron Avitzur^{6*}, Radu V Stan^{4*}, Aleixo M Muise^{1,2,3,10,§,*^}

Institutions

1. SickKids Inflammatory Bowel Disease Center and Cell Biology Program, Research Institute, Hospital for Sick Children, Toronto, ON, Canada.
2. Division of Gastroenterology, Hepatology, and Nutrition, Department of Pediatrics, University of Toronto, Hospital for Sick Children, Toronto, ON, Canada
3. Institute of Medical Science, University of Toronto, Toronto, ON, Canada
4. Department of Pathology, Department of Microbiology and Immunology, Geisel School of Medicine at Dartmouth, Hanover, NH 03756, USA
5. Genome Diagnostics, Department of Paediatric Laboratory Medicine The Hospital for Sick Children, Toronto, ON, Canada.
6. Group for Improvement of Intestinal Function and Treatment (GIFT), Hospital for Sick Children, Toronto, Ontario, Canada
7. Division of Pathology, The Hospital for Sick Children, Toronto, Canada
8. Division of Immunology, Department of Pediatrics, University of Toronto The Hospital for Sick Children, Toronto, Canada
9. Clinical and Metabolic Genetics, Department of Pediatrics, University of Toronto, Hospital for Sick Children, Toronto, ON, Canada
10. Department of Biochemistry, University of Toronto, Toronto, ON, Canada

§ interNational Early Onset Pediatrics IBD Cohort Study (www.NEOPICS.org)

and * Contributed equally

^ Address Correspondence to:

Aleixo Muise MD, PhD
555 University Ave.
The Hospital for Sick Children
Toronto, ON, Canada, M5G 1X8
Email: aleixo.muise@utoronto.ca
Phone: 416-813-7735
Fax: 416-813-6531

Grant Support: The authors thank the patient and family described here from Canada. The authors thank Karoline Fielder, from the Division of Pathology: Howard Rosenberg, Aina Tilups, Yew Meng Heng, Famida Spartare, Bernald Castro for technical assistance and Dr. Gino Somers for providing us with patient material. AE is supported by a Crohn's and Colitis Canada (CCC), Canadian Association of Gastroenterology (CAG), and Canadian Institute of Health Research (CIHR) Fellowship. CT is supported by the RESTRACOMP fellowship from the Research Institute of the Hospital for Sick Children, Toronto, Canada. Work in RVS lab was funded by NIH grants: CA175592, CA172983, CA023108 and S10OD010330. AMM is funded by a CIHR – Operating Grant (MOP119457) and by the Leona M. and Harry B. Helmsley Charitable Trust to study VEOIBD.

Conflict of Interest: The authors have no potential conflicts including financial, professional, or personal that are relevant to the manuscript.

Author contribution: AE, CT, SJD, RM, CH, JDS, carried out the investigations under the supervision of EC, CRM, DC, RVS, and AMM. YA, PW, CMR, RB and DC provided clinical care. AE with RVS and AMM wrote the manuscript with contributions from all authors.

Abstract

Background & Aims, Methods: Severe intestinal diseases observed in very young children are often the result of monogenic defects. We used whole exome sequencing (WES) to examine the genetic cause in a patient with a distinct severe form of protein losing enteropathy (PLE) characterized by hypoproteinemia, hypoalbuminemia, and hypertriglyceridemia.

Methods: WES was performed at the Centre for Applied Genomics, Hospital for Sick Children, Toronto, Canada. Exome library preparation was performed using the Ion Torrent AmpliSeq RDY Exome Kit. Functional studies were carried out based on the identified mutation.

Results: Using whole exome sequencing we identified a homozygous nonsense mutation (1072C>T; p.Arg358*) in the *PLVAP* (plasmalemma vesicle associated protein) gene in an infant from consanguineous parents who died at five months of age of severe protein losing enteropathy. Functional studies determined that the mutated PLVAP mRNA and protein were not expressed in the patient biopsy tissues, presumably secondary to nonsense-mediated mRNA decay. Pathological analysis showed that the loss of PLVAP resulted in disruption of endothelial fenestrated diaphragms.

Conclusions: PLVAP p.Arg358* mutation resulted in loss of PLVAP expression with subsequent deletion of the diaphragms of endothelial fenestrae leading to plasma protein extravasation, protein-losing enteropathy and ultimately death.

Keywords: Protein losing enteropathy, PLE, PLVAP, very early onset IBD, VEOIBD, IBD, endothelium, fenestrae, hypoproteinemia, hypoalbuminemia, and hypertriglyceridemia, monogenic diseases

Introduction

Protein losing enteropathy (PLE) is characterized by excessive loss of protein often due to the disruption of the integrity of the intestinal mucosal membrane or dilatation of the intestinal lymphatic system. Two broad categories of PLE have been described including mucosal injury causing excessive losses observed in Inflammatory Bowel Disease (IBD) and intestinal infections, and abnormalities of the lymphatic system observed in primary intestinal lymphangectasia^{1,2}. The latter encompasses a group of patients presenting with hypoalbuminemia, edema and dilatation of the lymphatics of the enteric system of unclear etiology.

Recently there has been growing interest into the genetic causes of severe intestinal phenotypes³. For example a novel Mendelian form of apoptotic enterocolitis caused by mutations in *TTC7A* was recently reported⁴; however, many infants with severe intestinal disease, including PLE, have yet to be identified causative genetic defects³. Here we use whole exome sequencing to identify a nonsense mutation in the *PLVAP* gene that results in a distinct severe form of PLE characterized by hypoproteinemia, hypoalbuminemia, and hypertriglyceridemia. The human form of PLVAP-deficiency is nearly identical to that observed in the *Plvap* knockout mice⁵ demonstrating the critical role of PLVAP in endothelial barrier function and intestinal homeostasis.

Methods

Subjects: All experiments were carried out with the approval of the Research Ethics Board (REB) at the Hospital for Sick Children. Informed consent to participate in research was obtained. A copy of the consent is available on the interNational Early Onset Paediatric IBD Cohort Study (NEOPICS) website at http://www.neopics.org/NEOPICS_Documents.html.

Samples from our patient carrying the PLVAP p.Arg358* mutation were obtained on two occasions while undergoing endoscopic investigation for severe protein losing enteropathy. Control samples from the duodenum or colon were obtained from patients undergoing evaluation of gastrointestinal symptoms where endoscopy and histology and the follow-up clinical impression were normal. A case of congenital Tufting Enteropathy as well as Microvillus Inclusion Disease initially presenting with protein losing enteropathy were assigned as duodenal

disease controls. Biopsies from a patient with IBD with inflamed areas in the colon served as a colonic disease control.

Next-generation sequencing: Whole-exome sequencing was performed at the Centre for Applied Genomics, Hospital for Sick Children, Toronto, Canada. Exome library preparation was performed using the Ion Torrent AmpliSeq RDY Exome Kit following the manufacturer's recommended protocol. In brief, 100ng of DNA quantified by Qubit DNA HS or BR assay was used in the target amplification under the following conditions: 99°C for 2 minutes, followed by 10 cycles at 95°C for 15 seconds and 60°C for 16 minutes, and final hold at 10°C. Incorporated primers sequences were partially digested using a proprietary method. Ion Torrent Proton adapters were ligated to the amplicons at 22°C for 30 minutes followed by 72°C for 10 minutes, and library was purified with Agencourt Ampure XT Beads. Libraries were quantified by qPCR and 7pM were used for sequencing on an Ion Torrent Proton Sequencer using a PI chip V2 following the manufacturer's protocol. All data were aligned to the hg19/GRCh37 reference genome and quality trimmed via Ion Torrent Suite Version 4.2.

Next-generation sequencing data analysis: SNP and Variation Suite Version 8.1 (Golden Helix) and VarSeq Version 1.1 (Golden Helix) were used. After importing the variant call files (VCF) of each member of the family trio (patient and parents), variants were organized by pedigree. Using the 1000 genomes Variant Frequencies (Phase 1), the Exome Aggregation Consortium Variant Frequency database Version 0.3 (Cambridge, MA) and the NHLBI Exome Sequencing Project V2 Exome Variant Frequencies, rare (Minor Allele Frequency <1%) variants were filtered. Variants were then classified according to whether they were deemed to be coding. Non-synonymous and unclassified variants were then scored using the database for non-synonymous functional predictions (dbNSFP 2.8), filtering out variants found to have no damaging score (Polyphen2, SIFT, MutationTaster, MutationAssessor, FATHMM). As well, dbNSFP scores variants with conservation scores (PhyloP and GERP++).

Sanger sequencing validation: Sanger sequencing was performed in the patient and his parents to validate the mutation identified by WES (c.1072C>T; p.Arg358*). The following primers were

used to sequence exons 2 and 3: Forward: AGCAAGTGTGAGATCAGCCT, and Reverse: GGCCAACATAGTGAAACCCC.

Constructs: The constructs generated are summarized below. All PLVAP constructs were cloned into the EcoRI and SalI sites of pIRES-hrGFP2a bicistronic vector (Agilent, San Diego, CA), allowing for expression of the target construct and humanized Renilla Green Fluorescent Protein (hrGFP). Two constructs encoding for the amino acids 1-357 of human PLVAP were generated, as a non-tagged version (labeled PLVAP R358*) or fused in frame with a string of 3 HA epitopes (labeled PLVAP 357-3xHA). The inserts were amplified by PCR using PFU polymerase (Agilent, San Diego, CA) and a previously reported⁶ full-length PLVAP (labeled PLVAP FL-3xHA) construct as a template. The following primers used were: sense

5'TGAATTCAAATGGGTCTGGCCATGGAGCAC3' and antisense:

5'AAAAGTCGACTGCAGGTGTCCAGGGCTGAGTTTC3' – for PLVAP 389-3xHA;

5'AAAAGTCGACCTTCCCTCCGCAGCACCCGC3' - for PLVAP 357-3xHA;

5'AAAAGTCGACTCATTCCCTCCGCAGCACCCGC3' - for PLVAP R358*;

5'AAAAGTCGACCCAGCGCTAGCTGGGTCTGCC3' - for PLVAP 348-3xHA;

5'AAAAGTCGACTCTGGCGTTGGAGGTCTGAG3' - for PLVAP 307-3xHA;

5'AAAAGTCGACAGGCCAATCCGAGCCCAG3' - for PLVAP 266-3xHA;

and 5'AAAAGTCGACCCGAGAGGGCTTGACCTTTTG3' - for PLVAP 225-3xHA. PCR products and vector were digested with EcoRI and SalI (NEB), gel purified, ligated using DNA ligase (Roche), introduced in TOP10 *E. coli* and selected on agar plates containing 100µg/ml Ampicillin. Positive clones confirmed by sequencing and restriction digestion were amplified using QiaPrep Endo-free columns (Qiagen, Germantown, MD).

PLVAP constructs generated and expected characteristics

PLVAP construct	Start PLVAP aa #	End PLVAP aa #	Protein length (aa)	Protein molecular weight (kDa)	Protein + N-glycosylation (10kDa)	3xHA (kDa)	Monomer (kDa)	Dimer (kDa)
FL-3xHA	1	442	442	50.59	60.59	3.50	64.09	128.18
389-3xHA	1	389	389	44.91	54.91	3.50	58.41	116.82
357-3xHA	1	357	357	41.16	51.16	3.50	54.66	109.32
R358*	1	357	357	41.16	51.16		51.16	102.32
348-3xHA	1	348	348	40.00	50.00	3.50	53.50	107.00
307-3xHA	1	307	307	35.48	45.48	3.50	48.98	97.96

266-3xHA	1	266	266	30.78	40.78	3.50	44.28	88.56
225-3xHA	1	225	225	25.00	35.00	3.50	38.50	77.00

Antibodies: Mouse anti-human PLVAP mAb⁷ (clone PAL-E, catalogue number ab8086), monoclonal antibody PAL-E specific for endothelium and mouse anti-human Plvap mAb Clone 174/2⁸ were purchased from Abcam. Hybridoma cells secreting PAL-E mAb was obtained from M. Kahn (U. Penn) and used to produce PAL-E mAb by BioXCell (Lebanon, NH). Anti-HA mAb clone HA.11 was used (Covance). Chicken anti-human PV1C pAb was previously described⁶. Goat anti-mouse IgG-HRP was from Biodesign, (Saco, ME), rabbit anti-chicken IgY-HRP was from Sigma and goat anti-mouse IgG-AlexaFluor 647 from Life Technologies (Eugene, OR).

Antibody labeling with fluorophores: Affinity purified primary antibodies mouse anti-PLVAP mAb clone PAL-E were labeled with Alexa 647 fluorophores (Life Technologies, Carlsbad, CA), as per manufacturer's instructions. The antibody-fluorophore conjugate was quality controlled for conjugation efficiency by spectroscopy (Varian Cary 50 BIO) and for aggregation by dynamic light scattering (Malvern Zetasizer Nano-ZS).

Cells: The spontaneously immortalized endothelial cell line EA.hy926 (CRL-2922, ATCC, Manassas, VA) or HEK293T cells were used for transfection experiments. Cells were cultured in DMEM with 10% FBS, penicillin and streptomycin.

Transfections: Equal numbers of cells were seeded at 70% confluence and cultured for 16-24h before transfection with various constructs using Lipofectamine LTX (Life Technologies), as per manufacturer's instructions. Controls consisted of non-transfected (NT) cells and cells transfected with empty pIRES-hrGFP2a vector (EV). In all experiments the transfection efficiency was ~10% for EA.hy926 cells and >80% for HEK293T cells, as determined by flow cytometry using hrGFP fluorescence as reporter.

Western blotting: Equal numbers of cells were seeded in 6 well plates (ThermoFisher) at 70% confluence and cultured for 16-24h before transfection with various constructs. Seventy-two hours post transfection cells were rinsed (2x, RT) with PBS, solubilized directly in 200µl non-

reducing Laemmli sample buffer for SDS PAGE, boiled 10 min and frozen at -20°C. Twenty-five µl of cell extracts were centrifuged resolved on 4-15% SDS PAGE using Criterion gels (BioRad), transferred to PVDF membranes and immunoblotted with either anti-human PLVAP mAbs clone 174/2 (2µg/ml, O/N, 4°C) or clone PAL-E (10 µg/ml, O/N, 4°C) or with chicken anti-human PV1C pAb (2µg/ml, O/N, 4°C) in 5% non-fat milk and 0.1% Tween-20 in PBS. Secondary detection was carried out by incubations (30min, RT) with 1µg/ml goat anti-mouse IgG-HRP or rabbit anti-chicken IgG-HRP, respectively, diluted in 5% non-fat milk and 0.1% Tween-20 in PBS. The signal was detected by chemiluminescence (Thermo-Fisher Pierce, Rockford, IL) followed by imaging using a G-Box gel imager (Syngene). Image data was exported as TIFF format and processed using Adobe Photoshop CS6 (Adobe Systems). The signal was inverted and the contrast and brightness adjusted using the auto levels function.

Flow cytometry: For flow cytometry, equal numbers of cells were seeded at 70% confluence in 24 well plates, in duplicate, and transfected the next day with various constructs. Seventy-two hours post transfection, cells were labeled (37°C, 30min, CO₂ incubator) while live and adherent with either 10µg/ml PAL-E mAb or 1µg/ml anti-HA mAb in full growth medium. Unbound primary antibody was washed (3x, RT) in DPBS with Calcium and Magnesium (Hyclone) and cells were chilled (5min, 10°C) to arrest endocytosis. Cells were incubated (30min, 10°C) with 3µg/ml goat anti-mouse IgG in ice cold 2% BSA in DPBS. Excess antibody was removed by washes (3x, on ice) in DPBS without Calcium and Magnesium and the cells were non-enzymatically dissociated from the plate using 200µl Cell Dissociation Solution (Sigma). The dissociation solution was removed and the cells were re-suspended in 1% BSA in PBS without Calcium and Magnesium and fluorescence was read on a FacsCalibur (Becton Dickinson) within Dartmouth DartLab flow cytometry core facility. Flow cytometry data was analyzed with either FlowLogic (Inivai Technologies, Mentone, Australia) or FlowJo (FlowJo LLC, Ashland, OR) software. Figures were assembled in either Adobe Photoshop or Adobe Illustrator CS6 software (Adobe).

Confocal Microscopy on transfected cells: Cells were seeded at 50% confluence on 1% gelatin coated 8 well Nunc™ Lab-Tek™ II Chambered Coverglass cultureware (Nunc, Thermo Scientific) and transfected with PLVAP FL-3xHA, PLVAP 389-3xHA, PLVAP 357-3xHA,

PLVAP R358* constructs or empty pIRES-hrGFP2a vector as control, as described above. Seventy two hours post transfection, live adherent cells were labeled as described above for flow cytometry, with either 10 μ g/ml PAL-E mAb or 1 μ g/ml anti-HA mAb, followed by Alexa 555-conjugated goat anti-mouse IgG for secondary detection. After the last wash following the secondary antibody the cells were fixed (30min, RT) with 4% paraformaldehyde in PBS, washed (3x5min, RT) in PBS, labeled (5min, RT) with 300nM 4',6-diamidino-2-phenylindole dihydrochloride (DAPI, Life Technologies, D1306) and washed (3x5min) in PBS. The cells were imaged while immersed in PBS. Imaging was done on a Zeiss 510Meta confocal microscope equipped with appropriate lasers (405nm, 488nm, 532nm) and filters, within the Dartmouth Norris Cotton Cancer Center microscopy facility. Acquired images were processed for brightness and contrast and analyzed using ImageJ and figures were mounted using Adobe Photoshop and Adobe Illustrator CS6.

EA.hy926 stable cell lines: The Zeocin resistance gene from \square Gal-Zeo vector (Invitrogen) was inserted in the vectors encoding for human PLVAP FL-3xHA, PLVAP 357-3xHA, PLVAP R358* constructs described above. The Zeocin resistance gene containing constructs were linearized and used to transfect EA.hy926 cells using Lipofectamine LTX (Invitrogen). Twenty-four hours post transfection, cells were switched to selection medium (growth medium containing 40 μ g/ml Zeocin (Invitrogen)) and under continuous selection for 4 weeks when the cells were sorted on double hrGFP and anti-PV1 PAL-E mAb positivity, using a FACS Aria sorter (Becton Dickinson). Mixed clonal populations were further used for determination of diaphragm formation by electron microscopy.

Electron microscopy: Patient duodenal biopsy tissue was fixed (1h, RT) by immersion in a fixative consisting of 2% glutaraldehyde and 3% paraformaldehyde in sodium cacodylate buffer, pH 7.2 and further processed (1h, on ice, in dark) through 1% OsO₄ post-fixation, incubated (1h, RT, in dark) in 2% uranyl acetate, dehydrated and embedded in LX-112 resin (Ladd Research Industries, Williston, VT). Thirty nanometer thick sections were obtained using a Leica EM UC6 microtome and an ultrasonic diamond knife (EMS Diasum) and examined and recorded under a Jeol 1010 electron microscope using a bottom mount AMD camera, within Dartmouth College EM facility.

Histological stains: Paraffin embedded tissue sections were deparaffinized using Xylene and afterwards dehydrated with graded ethanols. Next, slides were stained for 5 minutes with Hematoxylin and Eosin (Thermo Scientific). After dehydration of the tissue, sections were mounted with Entellan mounting medium (EMD-Millipore). For periodic acid-Schiff (PAS) cytochemistry, dehydrated sections were incubated in 0.5 % periodic acid solution (Sigma Aldrich) for 15 minutes at RT. Afterwards, the tissue was washed twice for 2 minutes with deionized water and incubated for 5 minutes in Schiff's reagent solution (Sigma Aldrich) in darkness. Next, sections were washed for 5 minutes at room temperature and counterstained with Hematoxylin solution (Thermo Scientific). Finally, slides were rehydrated and mounted with Entellan. Photomicrographs were taken using a Leica Inverted Light Microscope and adapted for brightness, contrast and pixel size using Adobe Photoshop CS5 Version 12.0 or Adobe Photoshop Illustrator CS6.

Immunofluorescence on biopsy samples: Intestinal biopsies from both the patient and controls were fixed either with 10% Formaldehyde without Methanol and embedded in paraffin or directly processed with O.C.T (Optimal Cutting Temperature) Compound (Tissue-Tek) for frozen sections. For paraffin embedded sections, paraffin was removed using Xylene, and afterwards rehydrated with different percentages of ethanol. An antigen retrieval step was performed with high pressure-cooking with 1 mM EDTA at a pH of 9 with 0.05 % Tween 20. Frozen sections were fixed with ice-cold Methanol at -20°C for 5 minutes and shortly washed with 1x PBS without Ca and Mg. Afterwards, slides were blocked for 1 hour at room temperature with 5 % BSA in 1x PBS without Ca and Mg containing 15 % goat serum. Primary antibody incubation was performed overnight at 4°C . On the following day, stained slides were washed 3 times for 10 minutes with 1x PBS without Ca and Mg. Secondary antibody incubation was performed at room temperature and in darkness for 1 hour, and slides were washed afterwards 3 times for 10 minutes in darkness. Next, nuclear counterstaining with Hoechst 33342 Fluorescence Stain (Thermo Scientific) was performed at a dilution of 1:15.000. Finally sections were mounted overnight with Vectorshield fluorescence mounting medium (Vector Labs). Rabbit-polyclonal anti-ZO1 (Abcam), mouse-monoclonal anti-beta catenin (BD Transduction Laboratories), mouse-monoclonal anti-PLVAP clone 174/2 (Abcam) and rabbit-polyclonal anti CD31 (Abcam) were

used as primary antibodies in a dilution of 1:100. ALEXA 568 goat anti-rabbit (Life Technologies) and ALEXA 488 goat-anti mouse (Life Technologies) served as secondary antibodies in a dilution of 1:500. ALEXA647-conjugated anti-PLVAP clone PAL-E mouse monoclonal antibody described above was used on methanol fixed frozen sections at a concentration of 10 µg/ml blocking solution. Photomicrographs of immunostained sections were taken with an Olympus IX81 inverted fluorescence microscope equipped with a Hamamatsu C9100-13 back-thinned EM-CCD camera and Yokogawa CSU X1 spinning disk confocal scan head. Images were adjusted for contrast and brightness using the Volocity 6.1.1 version software (Perkin Elmer). Images were then mounted using Adobe Photoshop CS5 Version 12.0 or Adobe Photoshop Illustrator CS6.

RNA detection by in situ hybridization on biopsy samples: RNA was detected in formalin fixed paraffin embedded biopsy tissue sections (10µm thick) from patient and controls by *in situ* hybridization using human PLVAP C1-RNA scope probes and RNA scope technology⁹, as per manufacturer's instructions (Advanced Cell Diagnostics, Hayward, CA). RNA scope detection was carried out at Dartmouth Norris Cotton Cancer Center Pathology Translational Research Laboratory core facility.

Results

Clinical History: Our patient was born at 36 weeks gestational age via C-section to consanguineous parents of Afghan descent. He presented to the Hospital for Sick Children at 8 days of life with secretory diarrhea, metabolic acidosis, lethargy, poor feeding and severe hyponatremia causing seizures. He developed hematochezia on day-of-life 9. On further examination, he was also found to have bilateral colobomas, undescended testis, mildly dysplastic kidneys bilaterally, low set ears and micrognathia.

Most notable on laboratory examination was his consistently undetectable (<10g/L) albumin that did not respond to repeated infusions (19g/L was the highest level drawn during a continuous albumin infusion). However, there was no evidence of proteinuria, including normal urea, creatinine, transaminases, cortisol and urine electrolytes. All immunoglobulins (IgG, IgA, IgE

and IgD) were low or undetectable, except for IgM, which was normal. TSH was severely elevated (31.1mIU/L), and free T4 was undetectable (<5.1pmol/L). Lipid profile analysis showed a markedly elevated triglyceride level (4.3-10.3mmol/L), with a normal cholesterol and HDL level noted (Supplemental Table 1).

Over the next two months of life, he developed enteroviral and rhinoviral upper respiratory tract infections. He persistently had severe anasarca and was found to have venous thrombosis in multiple locations. After developing a *Klebsiella oxytoca* urinary tract infection, he developed ascites and acute breathing difficulty, followed by pericardial effusion that required a pericardial drain placement. Shortly before he was 5 months old, he developed Coagulase negative *Staphylococcus aureus* sepsis, resulting in decompensation, multi-organ failure and death at 136 days old. No post-mortem examination was performed at the family's request.

Histopathology: Due to the severe ongoing diarrhea, upper and lower endoscopy was performed at 2 months and 3.5 months of age and showed severely pale edematous duodenum, edematous stomach and normal colon. Hematoxylin and eosin (HE) and periodic acid–Schiff (PAS) staining demonstrated prominent, diffuse edema in the interstitium with the absence of epithelial architectural distortions, signs of lymphangectasia, or signs of acute inflammation (Figure 1A and B). Immunohistochemistry analysis showed normal basolateral epithelial cell adhesion molecule (EpCAM) and apical CD10 expression and localization patterns. No apparent changes in interstitial regulatory T-cells (Tregs) expressing FOXP3 (Supplemental Figure 1) As well, tight junctions and adherens junctions were normal (Supplemental Figure 2A-B) Transmission electron microscopy (TEM) showed normal apical brush border microvilli with no histopathological features of congenital Tufting enteropathy (CTE), Microvillus inclusion disease (MVID) or Immune dysregulation, polyendocrinopathy, enteropathy, X-linked (IPEX) syndrome (Figure 1B). Patient derived enteroids demonstrated normal growth and morphology (data not shown).

Genetic Analysis: Whole exome sequencing using the Ion Torrent Proton platform of the patient and parents (Figure 2A) identified 49,722 variants (Figure 2B). As the patient's parents were consanguineous, we focused on rare damaging homozygous variants and identified 17 variants (Supplemental Table 2). Based on known protein function, expression profiles, animal models,

and conservation scoring, this list was narrowed down to a single candidate gene, *PLVAP* (plasmalemma vesicle associated protein). The identified homozygous mutation in exon 3 of *PLVAP* resulted in a premature stop codon (c.1072C>T; p.Arg358*) (Figure 2C). The *PLVAP* c.1072C>T mutation is extremely rare with only 1 heterozygote individual identified from over 121,000 sequenced (estimated minor allelic frequency of 8.2e-06; <http://exac.broadinstitute.org/variant/19-17476202-G-A>). *PLVAP* is a cationic, integral membrane glycoprotein that is specifically expressed in endothelial cells¹⁰. *PLVAP* forms homodimers⁶, and plays a critical role in the formation of the diaphragms of caveolae and fenestrae/transendothelial channels^{5, 6, 11}. *PLVAP* positive diaphragms of fenestrated capillaries are essential for the maintenance of blood composition^{5, 12}.

Functional Analyses: To determine if the diaphragms in the intestinal fenestrated capillaries were disrupted in our patient, we performed Transmission Electron Microscopy (TEM) with ultrathin (30 nanometer) sections of the small intestinal biopsy. We observed an absence of diaphragms in both the fenestrae and caveolae of the endothelial cells of vessels in the intestinal biopsies (Figure 3A). Additionally, general edema of the tissue (Figure 1B, right panel) and accumulation of lipid droplets in the interstitial area near the endothelium were also observed (Figure 3B). These TEM findings are identical to those previously described in the *Plvap* knockout mice^{5, 13, 14}.

The identified *PLVAP* 1072C>T p.Arg358* mutation is predicted to introduce a premature stop codon and cause an 84 C-terminal amino acid truncation including part of the *PLVAP* coil-coiled domain and the proline-rich region (PRR) (Figure 2B). Because mRNAs with premature stop codons can be targeted for degradation^{15, 16}, we tested whether the mutant *PLVAP* p.Arg358* mRNA and protein were expressed in patient samples. Quantitative *in situ* hybridization with *PLVAP* specific probes using RNAscope technology^{9, 17} showed a drastic reduction in *PLVAP* mRNA expression in patient biopsy tissue (Figure 3C, right panel) whereas the signal was readily detected in biopsies from normal and disease control patients (Figure 3C left and middle panel).

To confirm these findings at the protein level, we first identified an antibody capable of detecting the truncated *PLVAP* p.Arg358* protein. Using a battery of *PLVAP* truncation mutants (Figure

4A) and previously characterized anti-human PLVAP antibodies directed against its extracellular domain (anti-PV1C pAb⁶, clone 174/2⁸, clone PAL-E^{7,8}), we determined that anti-PLVAP mAb clone PAL-E recognized an epitope between PLVAP amino acids 225-307 (data not shown) and therefore was able to detect PLVAP p.Arg358* protein (Figure 4B, *top panel*), whereas clone 174/2 did not, as it recognized an epitope situated between amino acids 358-389 (Figure 4B, *middle panel*). As previously reported, PAL-E had a much higher affinity for the dimeric form of the PLVAP FL^{7,8}, which we found to be also true for PLVAP truncation mutants (Figure 4B, *top panel*). As expected, anti-hPV1C pAb raised against the last 12 amino acids of human PLVAP recognized only full length PLVAP (Figure 4B, *bottom panel*). To shore up the RNA data, we carried out immunofluorescence with anti-PLVAP clone PAL-E directly conjugated to fluorophores (as means to decrease possible artefacts due to secondary antibody detection) and anti-CD31 antibodies as a marker for endothelial cells¹⁸. In concordance with the RNAscope results, PLVAP protein expression was drastically reduced in patient biopsy tissue (Figure 3D-F and Supplemental Figure 2C-D).

These results prompted us to test the possibility of additional mechanisms contributing to PLVAP p.Arg358* protein degradation such as failure to pass ER quality control or defective trafficking due to improper folding and/or glycosylation¹⁹. Our data demonstrated that both PLVAP R358* and PLVAP 357-3xHA were translated and readily expressed from a cDNA in spontaneously immortalized human Ea.hy956 endothelial cells (Figure 4B) and other cell types in culture (not shown). PLVAP R358* and PLVAP 357-3xHA proteins formed homodimers, as shown by immunoblotting of proteins resolved in reducing and non-reducing conditions with either PAL-E or anti-HA mAbs (Figure 4B-D). Both constructs were N-glycosylated, demonstrating an apparent drop in molecular weight of appropriate size (~10kd for all monomers) upon treatment with PNGase F, an endoglycosidase purified from *Flavobacterium meningosepticum* that removes all N-linked glycans except those containing core α 1-3 Fucose²⁰, (Figure 4C-D). Last, both PLVAP R358* and PLVAP 357-3xHA constructs were efficiently trafficked to the plasma membrane, as demonstrated by both confocal microscopy (Figure 5A) or flow cytometry (Figure 5B-C) using PAL-E or anti-HA antibodies on live non-permeabilized cells. These data show that the truncated PLVAP R358* demonstrates similar biochemical and cell biological behaviour to full length PLVAP and improper folding or glycosylation is not a likely a cause for the lack of

PLVAP p.Arg358* protein in patient samples. Together, the data strongly suggest that PLVAP 1072C>T p.Arg358* mutation results in a *de facto* PLVAP knockout due to efficient degradation of mutant RNA.

Discussion

PLVAP encodes an endothelial specific type II integral membrane protein forming homodimers thought to create the radial fibrils / spokes in the ring-and-spoke structure of the diaphragms of endothelial fenestrae, TEC and caveolae²¹. By this model, PLVAP C-termini would form the center / hub of the diaphragm by protein-protein interactions with so far unknown partners²¹ (Figure 6). Interestingly, the clinical and pathological findings in our patient are nearly identical to the previously described *Plvap* knockout mouse models where *Plvap*-deficiency results in loss of diaphragms and a sieving vascular leakage of plasma proteins characterized by hypoproteinemia, edema and hypertriglyceridemia with extracellular lipid deposits^{5,13,14}.

Electron microscopic observation of our patient biopsies demonstrated a complete lack of diaphragms in the fenestrae and caveolae of endothelial cells of all the capillaries in the duodenum villi examined. Besides the clinical presentation (as described below), histopathological and electron microscopic observation detected other signs such as tissue edema, endothelial thickening and extracellular lipid deposition that were previously reported in *Plvap* knockout mice^{5, 13, 14}. These data suggested that the truncated mutant PLVAP was either not expressed or was incapable of forming diaphragms (Figure 6).

The identified PLVAP 1072C>T p.Arg358* mutation introduces a premature stop codon in exon 3 resulting in a C-terminal truncation of 84 aa if the mutant mRNA would be stable and translated into protein. The location of the premature stop codon on PLVAP exon 3 (the stop codon of full length PLVAP mRNA is on exon 6) at more than 100 nucleotides from the nearest exon-exon junction makes the mutant PLVAP p.Arg358* mRNA a good candidate for degradation via nonsense mediated decay (NMD)^{15, 16}. These and the EM data prompted us to test whether the mutant mRNA and protein were expressed in patient samples.

Using a robust quantitative in situ hybridization technology (RNAscope) we show that the patient's intestinal biopsy samples have drastically reduced PLVAP mRNA signal. The decreased mRNA signal is likely not the result of the hybridization mismatch between PLVAP RNAscope probes and the single nucleotide mutated mRNA, as RNAscope probes consist of twenty sets of individual 20 nucleotide probes spanning approximately 1kb of the target mRNA. Our data show that this likely is not a technical artefact due to the degradation of RNA, as intestinal biopsies from disease controls collected and processed by the same stringent protocol show very robust signal. Moreover, all of the 4 different biopsies (duodenum and colon at two time points) from the patient show drastically decreased PLVAP mRNA signal. Most compellingly, the decreased expression of mutant mRNA was strongly supported by data showing that PLVAP protein is not expressed in the patient intestine biopsies, whereas clear PLVAP signal was obtained in the endothelial cells of vessels in biopsies from normal and diseased controls. The lack of mutant PLVAP p.Arg358* protein expression was not due to problems in protein folding in ER and subsequent degradation, as PLVAP p.Arg358* formed homodimers of expected molecular size. Additionally, PLVAP p.Arg358* underwent N-glycosylation similar to the normal full length PLVAP, suggesting progression through the Golgi apparatus, and was trafficked correctly to the cell surface when transiently or stably expressed in endothelial cells or other mammalian cells. Thus the identified mutation results in a *de facto* PLVAP knockout likely due to mRNA instability.

Here, we describe the first human PLVAP mutation resulting in a severe fatal sieving hypoproteinemia and enteropathy. Deletion of fenestral diaphragms causes leakage of plasma proteins into the interstitium of organs provided with fenestrated capillaries (intestine, pancreas, adrenals) and from there into the peritoneal cavity and into the intestine lumen, but not in organs with continuous endothelium (heart, muscle, lung)^{8,10}. In our patient a number of plasma proteins were severely decreased including albumin (65-70 kDa), IgA, D, G and E (150 kDa), ceruloplasmin (151 kDa) and thyroxine binding globulin (54 kDa) while IgM (755 kDa) was normal as a result of selected loss of proteins based on their size. Therefore the hypoproteinemia, hypoalbuminemia, and hypertriglyceridemia observed in our patient occurred due to loss of fenestral diaphragms in the intestine⁵. In contrast, the absence of PLVAP positive fenestral diaphragms in liver sinusoids or glomerulus²² explains the lack of proteinuria and the normal liver

function found in our patient. The abnormal lipid composition in the described patient resembled the lipid profile found in the *Plvap* knockout mice⁵, although in general the severity of the changes was less in the patient compared to the mouse model. HDL-cholesterol concentrations were within the reference values in our patient but were found to be lower in the mouse model. Triglyceride concentrations were up to 10-fold higher in the patient, but >20 fold higher in the knockout mice compared to wild type mice, which does indicate a difference in metabolic disease severity. Based on their findings of similar levels of gene expression of apoB mRNA levels they suggested that the hypertriglyceridemia was not related to an enhanced very low-density lipoprotein (VLDL) secretion. In support of this hypothesis is the finding that in nutritionally induced hypoproteinemia (*i.e.* severe acute malnutrition) VLDL secretion appears not to be affected²³. *Plvap* knockout mice exhibited a very slow decrease of VLDL levels upon fasting⁵, suggesting that hypertriglyceridemia was most likely due to impaired lipoprotein lipase function, which is an essential enzyme that hydrolyzes lipoprotein bound triglycerides. In addition, triglyceride-rich lipoprotein particles such as VLDL (25-90 nm), chylomicrons (1000 nm) and chylomicron remnants (30-50 nm) are larger than the molecular diameter cut-off (~30 nm) resulting from a loss of diaphragms and persistence of the capillary basement membrane. Unfortunately, we were unable to measure lipoprotein lipase function in our affected patient to support the hypothesis that hypertriglyceridemia is related to low levels of lipoprotein lipase in loss of PLVAP in humans.

The pathogenesis of the hypoalbuminemia observed in our PLVAP-deficiency patient was significantly different from the two broad categories that are commonly used to describe PLE^{1,2}. Although our patient initially presented with bloody diarrhea, there was no histological evidence of mucosal injury that caused excessive protein losses observed in ulcerative colitis²⁴, Crohn's Disease²⁵ and TTC7A-deficiency⁴. We also did not identify any abnormalities of the lymphatic system that are observed in primary intestinal lymphangiectasia²⁶. In contrast to other congenital enteropathies such as Microvillus Inclusion Disease (MVID) or congenital Tufting Enteropathy (CTE), the primary defect is not harbored by intestinal epithelial, but endothelial cells²⁷⁻³⁰. Duodenal enterocytes in the patient with PLVAP mutation showed normal brush border morphology, indicating that the intestinal barrier function is not primarily affected. Therefore the intractable secretory diarrhea observed in our PLVAP patient was not caused by malabsorption

due to defective brush border, but as a consequence of protein loss and reduced colloid osmotic pressure due to leaky fenestrated capillaries in the intestine. The precise molecular mechanism of epithelial barrier failure and resultant PLE are not known.

In summary, we have identified a homozygous nonsense mutation in the PLVAP gene in our patient who developed severe PLE that was nearly identical to the phenotype observed in the *Plvap* knockout mice. In both mice and humans, the loss of functional PLVAP results in disruption of fenestral diaphragms in the intestinal vasculature that is characterized by hypoproteinemia, hypoalbuminemia, hypertriglyceridemia and premature death. Further work in animals modeling the human PLVAP mutation should shed light on the molecular mechanism of PLVAP down regulation, as well as the molecular mechanisms resulting in epithelial barrier disruption prompting interventional strategies.

References

1. Braamskamp MJ, Dolman KM, Tabbers MM. Clinical practice. Protein-losing enteropathy in children. *Eur J Pediatr* 2010;169:1179-85.
2. Umar SB, DiBaise JK. Protein-losing enteropathy: case illustrations and clinical review. *Am J Gastroenterol* 2010;105:43-9; quiz 50.
3. Uhlig HH, Schwerdt T, Koletzko S, et al. The Diagnostic Approach to Monogenic Very Early Onset Inflammatory Bowel Disease. *Gastroenterology* 2014.
4. Avitzur Y, Guo C, Mastropaolo LA, et al. Mutations in tetratricopeptide repeat domain 7A result in a severe form of very early onset inflammatory bowel disease. *Gastroenterology* 2014;146:1028-39.
5. Stan RV, Tse D, Deharvengt SJ, et al. The diaphragms of fenestrated endothelia: gatekeepers of vascular permeability and blood composition. *Dev Cell* 2012;23:1203-18.
6. Stan RV. Multiple PV1 dimers reside in the same stomatal or fenestral diaphragm. *Am J Physiol Heart Circ Physiol* 2004;286:H1347-53.
7. Schlingemann RO, Hofman P, Anderson L, et al. Vascular expression of endothelial antigen PAL-E indicates absence of blood-ocular barriers in the normal eye. *Ophthalmic Res* 1997;29:130-8.
8. Niemela H, Elima K, Henttinen T, et al. Molecular identification of PAL-E, a widely used endothelial-cell marker. *Blood* 2005;106:3405-9.
9. Wang F, Flanagan J, Su N, et al. RNAscope: a novel in situ RNA analysis platform for formalin-fixed, paraffin-embedded tissues. *J Mol Diagn* 2012;14:22-9.
10. Stan RV, Kubitzka M, Palade GE. PV-1 is a component of the fenestral and stomatal diaphragms in fenestrated endothelia. *Proc Natl Acad Sci U S A* 1999;96:13203-7.
11. Ioannidou S, Deinhardt K, Miotla J, et al. An in vitro assay reveals a role for the diaphragm protein PV-1 in endothelial fenestra morphogenesis. *Proc Natl Acad Sci U S A* 2006;103:16770-5.
12. Stan RV, Tkachenko E, Niesman IR. PV1 is a key structural component for the formation of the stomatal and fenestral diaphragms. *Mol Biol Cell* 2004;15:3615-30.
13. Herrnberger L, Ebner K, Junglas B, et al. The role of plasmalemma vesicle-associated protein (PLVAP) in endothelial cells of Schlemm's canal and ocular capillaries. *Exp Eye Res* 2012;105:27-33.
14. Herrnberger L, Seitz R, Kuespert S, et al. Lack of endothelial diaphragms in fenestrae and caveolae of mutant Plvap-deficient mice. *Histochem Cell Biol* 2012;138:709-24.
15. Miller JN, Pearce DA. Nonsense-mediated decay in genetic disease: friend or foe? *Mutat Res Rev Mutat Res* 2014;762:52-64.
16. Popp MW, Maquat LE. Organizing principles of mammalian nonsense-mediated mRNA decay. *Annu Rev Genet* 2013;47:139-65.
17. Monyer H, Hartley DM, Choi DW. 21-Aminosteroids attenuate excitotoxic neuronal injury in cortical cell cultures. *Neuron* 1990;5:121-6.
18. Deharvengt SJ, Tse D, Sideleva O, et al. PV1 down-regulation via shRNA inhibits the growth of pancreatic adenocarcinoma xenografts. *J Cell Mol Med* 2012;16:2690-700.
19. Tannous A, Pisoni GB, Hebert DN, et al. N-linked sugar-regulated protein folding and quality control in the ER. *Semin Cell Dev Biol* 2014.
20. Plummer TH, Jr., Tarentino AL. Purification of the oligosaccharide-cleaving enzymes of *Flavobacterium meningosepticum*. *Glycobiology* 1991;1:257-63.
21. Tse D, Stan RV. Morphological heterogeneity of endothelium. *Semin Thromb Hemost* 2010;36:236-45.

22. Clementi F, Palade GE. Intestinal capillaries. I. Permeability to peroxidase and ferritin. *J Cell Biol* 1969;41:33-58.
23. Badaloo AV, Forrester T, Reid M, et al. Nutritional repletion of children with severe acute malnutrition does not affect VLDL apolipoprotein B-100 synthesis rate. *J Nutr* 2012;142:931-5.
24. Ungaro R, Babyatsky MW, Zhu H, et al. Protein-losing enteropathy in ulcerative colitis. *Case Rep Gastroenterol* 2012;6:177-82.
25. Baert D, Wulfrank D, Burvenich P, et al. Lymph loss in the bowel and severe nutritional disturbances in Crohn's disease. *J Clin Gastroenterol* 1999;29:277-9.
26. Vignes S, Bellanger J. Primary intestinal lymphangiectasia (Waldmann's disease). *Orphanet J Rare Dis* 2008;3:5.
27. Davidson GP, Cutz E, Hamilton JR, et al. Familial enteropathy: a syndrome of protracted diarrhea from birth, failure to thrive, and hypoplastic villus atrophy. *Gastroenterology* 1978;75:783-90.
28. Muller T, Hess MW, Schiefermeier N, et al. MYO5B mutations cause microvillus inclusion disease and disrupt epithelial cell polarity. *Nat Genet* 2008;40:1163-5.
29. Thoeni C, Amir A, Guo C, et al. A novel nonsense mutation in the EpCAM gene in a patient with congenital tufting enteropathy. *J Pediatr Gastroenterol Nutr* 2014;58:18-21.
30. Sivagnanam M, Mueller JL, Lee H, et al. Identification of EpCAM as the gene for congenital tufting enteropathy. *Gastroenterology* 2008;135:429-37.

Figure Legends

Figure 1: Low power light and electron microscopy shows edema and absence of intestinal structural defects in PLVAP p.R358* mutation. **A.** HE and PAS stain of the duodenum from a control (left) and the PLVAP p.R358* patient (right). HE and PAS stain show prominent interstitial edema in the duodenum (shown by the pale interstitium in the villus area). Scale bars - 200 μm **B.** TEM analysis of the duodenum from a control (left) and the PLVAP p.R358* patient (right) showing no abnormalities within the ultrastructure of the enterocyte epithelium. Scale bars - 2 μm .

Figure 2: Identification of a PLVAP (plasmalemma vesicle associated protein) Mutation in an infant with severe Protein Losing Enteropathy. **A.** Pedigree. **B.** Whole Exome Sequencing variant filtration algorithm showing the variants identified in the patient and parents (listed in Supplemental table 2). **C.** Domain, gene and mRNA view. Gray arrows show glycosylation sites. The identified mutation (red), coil-coiled regions (pink), trans-membrane regions (black) and a proline rich region (green) are noted.

Figure 3: PLVAP p.R358* mutation causes loss of the diaphragms of endothelial fenestrae and caveolae and severely decreased levels of mRNA and protein. **A.** Electron micrographs of small intestinal biopsies from control (left panel) and PLVAP p.R358* patient (right panel). Fenestrae and caveolae of the mutant endothelial cells do not have diaphragms (*arrows*) whereas diaphragms are readily present in normal endothelial cells (*). Scale bars - 500 nm **B.** Electron micrographs of PLVAP p.R358* patient duodenum biopsy, showing extracellular lipid droplets (black arrows). The image on the right is a higher magnification of the indicated area in the left micrograph. Scale bars: left - 2 μm , right - 1 μm . **C.** Detection of human PLVAP mRNA (blue-green staining) using RNAscope probes in duodenal biopsies from a normal control (left), a patient with congenital tufting enteropathy (CTE, middle), and PLVAP p.R358* patient (right). The general architecture of the tissue is revealed by hematoxylin counterstain. Scale bars – 100 μm **D-F.** Nuclei were stained with Hoechst (blue). Disease controls used are Microvillous Inclusion Disease (MVID) in D, Congenital Tufting Enteropathy (CTE) in E, and active colonic Inflammatory Bowel Disease (IBD) in F. Scale bars (D-F) - 100 μm . **D.** Multiplex immunofluorescence with anti-PLVAP (clone PAL-E)-Alexa 647 (purple) and anti-CD31

(yellow) on methanol fixed frozen sections of duodenal biopsies from normal control (left), control MVD patient (middle) and PLVAP p.R358* patient (right). Hoechst stains nuclei in blue. **E-F.** Multiplex immunofluorescence with anti-PLVAP (clone 174/2) (green) and anti-CD31 (red) on FFPE sections from normal control (left), control disease patient (middle) and PLVAP p.R358* patient (right). Sections were obtained from duodenum (E) and colon (F) biopsies.

Figure 4: Functional studies of mutated forms of PLVAP. **A.** Schematic constructs of various truncation mutations generated. N-Glyc – N-glycosylation, CC- coiled coil domain, PRR – proline rich region, TM – transmembrane region, 3xHA – trio tandem of HA epitopes, downward orange lines mark the position of cysteines. **B.** PLVAP R358* forms homodimers detected by the anti-PLVAP mAb clone PAL-E. Immunoblotting analysis of 10% (top) or 4-20% (middle and bottom) SDS-PAGE resolved lysates of Ea.hy926 cell transfected with empty vector (EV) or with human PLVAP full length-3xHA (FL), human PLVAP 1-389-3xHA (389), human PLVAP 1-357-3xHA (357-3xHA) or human PLVAP R358* truncation constructs. The membranes have been probed with three available anti-human PLVAP antibodies recognizing different epitopes: PAL-E - mouse anti-human PLVAP mAb clone PAL-E (*top panel*), mouse anti-human PLVAP mAb clone 174/2 (*top panel*), and anti-hPV1C - chicken anti-human PV1C pAb. While Ea.hy926 are devoid of endogenous PLVAP, bands of expected molecular weight were readily detected by all three antibodies in PLVAP FL-3xHA transfected cell lysates in reducing (r, ~63kDa) and nonreducing (n, ~126 kDa) conditions (corresponding to PLVAP FL-3xHA monomers or homodimers, respectively). The only antibody that recognized PLVAP R358* and PLVAP 357-3xHA was PAL-E. **C.** PLVAP R358* is N-glycosylated. Immunoblotting with PAL-E (top) or anti-HA mAb (bottom) of total cellular proteins from Ea.hy926 endothelial cells expressing PLVAP truncation constructs treated (+) or not (-) with PNGase F to remove N-glycans. The proteins were resolved by nonreducing 8% and reducing 4-20% SDS-PAGE, respectively. Controls consisted of non-transfected (NT) or empty vector (EV) transfected Ea.hy926 cells. PAL-E antibody recognized bands of an appropriate size corresponding to the glycosylated and de-glycosylated forms of PLVAP FL-3xHA and -389-3xHA and R358* truncations constructs (see Supplemental Methods). **D.** Immunoblotting with mouse anti-HA mAb of total cellular proteins from endothelial cells expressing PLVAP truncation constructs treated (+) or not (-) with PNGase F to remove N-glycans resolved by

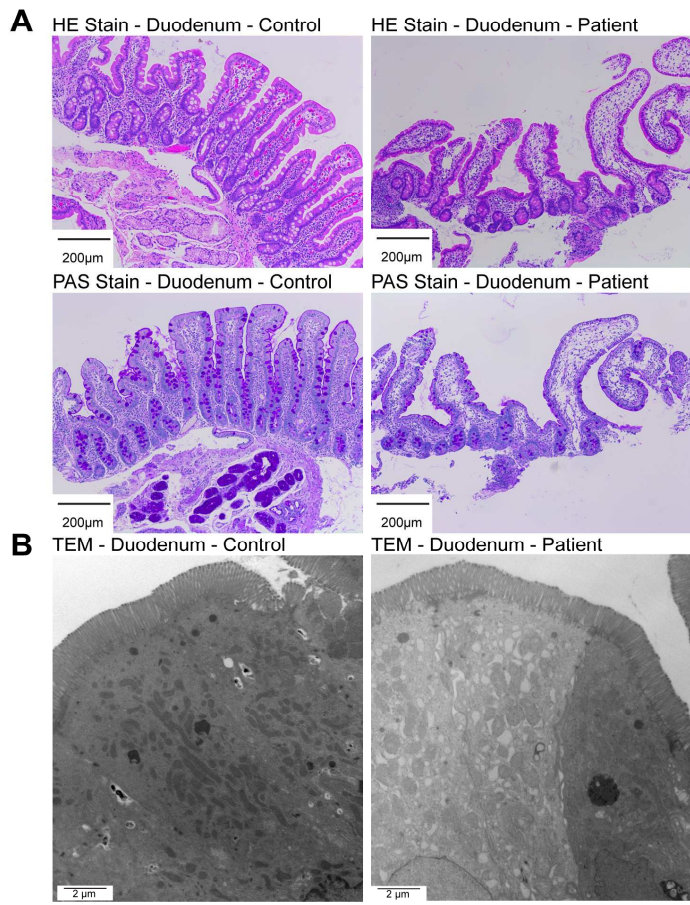
reducing 8% SDS-PAGE. A ~15kDA drop was detected in 357-3xHA upon PNGase F treatment (+).

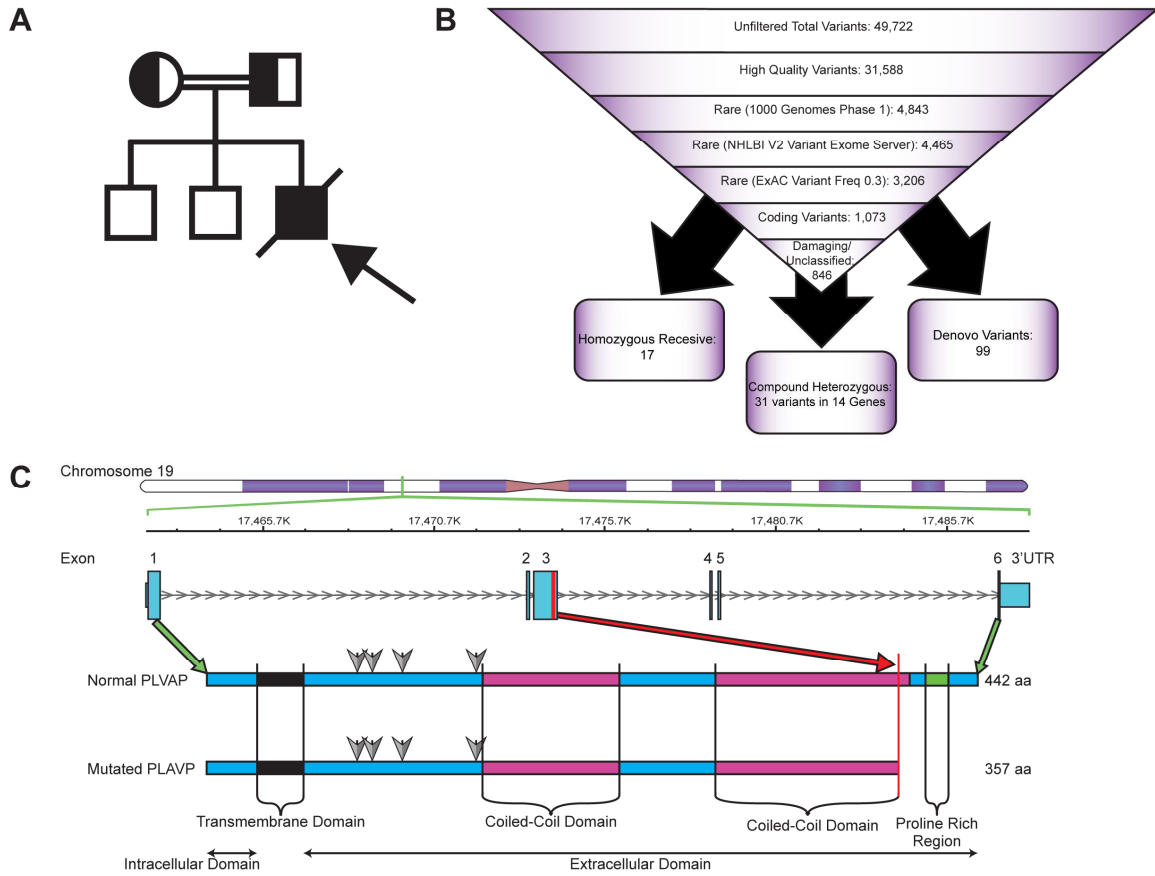
Figure 5: PLVAP R358* is trafficked to the plasma membrane of endothelial cells. A.

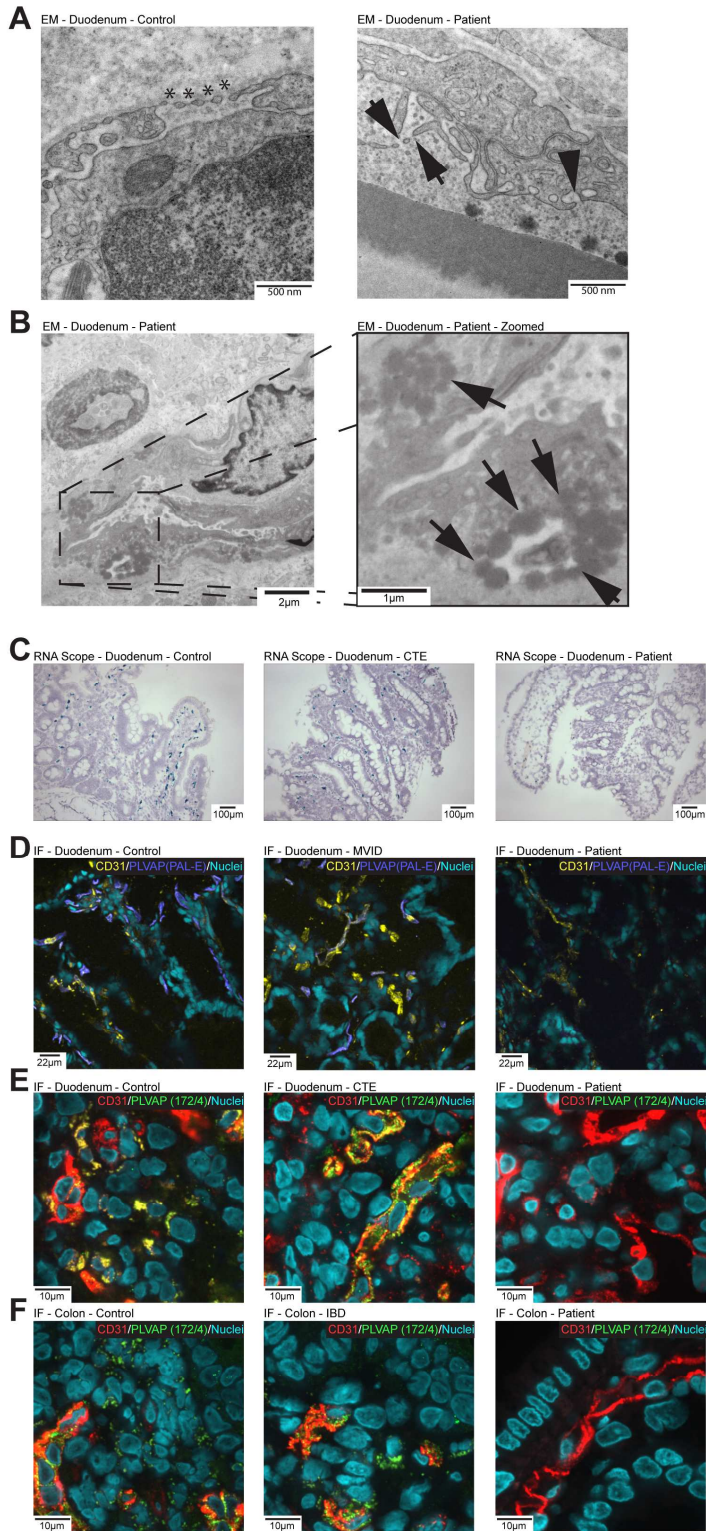
Confocal microscopy demonstrating the expression of PLVAP R358* on the surface of live endothelial cells. Live transfected cells were labeled with PAL-E mAb followed by goat anti mouse IgG-AlexaFluor 647 (red). The cells were transfected with bicistronic vectors encoding for full length PLVAP-3xHA (FL), PLVAP 389-3xHA (1-389), PLVAP R358* (R358*) or empty vector (EV). Transfected cells were detected by hrGFP fluorescence (green). Scale bars – 50µm. **B.** Flow cytometric analysis of Ea.hy962 cells transfected with full length PLVAP (FL-HA) (*pink trace*), PLVAP R358* (R358*) (*orange trace*) and PLVAP 357-3xHA (357 HA) (*green trace*). Controls consisted of non-transfected Ea.hy962 cells (black trace) or Ea.hy962 cells transfected with empty vector (EV) (grey trace). PLVAP constructs were expressed from bicistronic vectors also encoding for hrGFP as described in methods. *Left* – gating on hrGFP positive cells; *Right* – PAL-E mAb signal in hrGFP positive cells. **C.** Flow cytometric analysis of Ea.hy962 cells transfected with full length PLVAP (FL-3xHA), PLVAP R358* (R358*) and PLVAP 357*-3xHA (1-357HA) (green trace). Controls consisted of non-transfected Ea.hy962 cells (black trace) or Ea.hy962 cells transfected with empty vector (EV)(grey trace). PLVAP constructs were expressed from bicistronic vectors also encoding for hrGFP. Cells were labeled with either PAL-E mAb (two left columns) or with anti-HA mAb (two right columns). In each case *Left* – gating on hrGFP positive cells; *Right* – gating on PAL-E or anti-HA mAb signal in hrGFP positive cells.

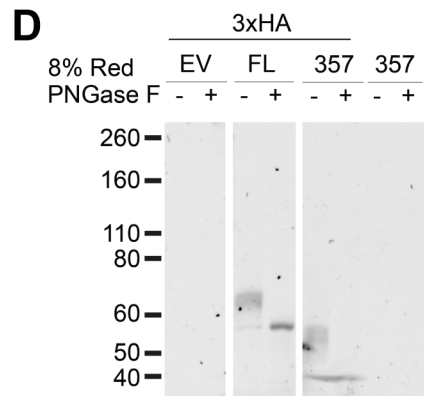
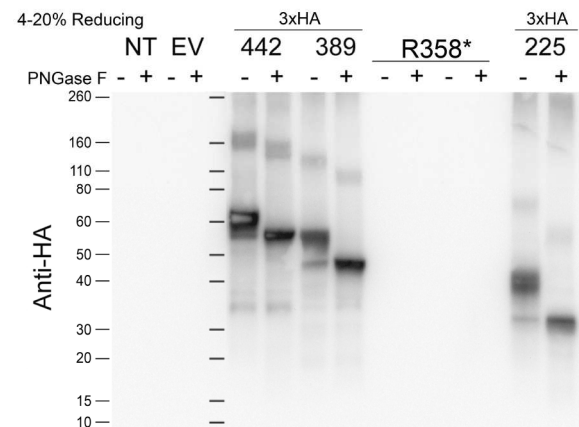
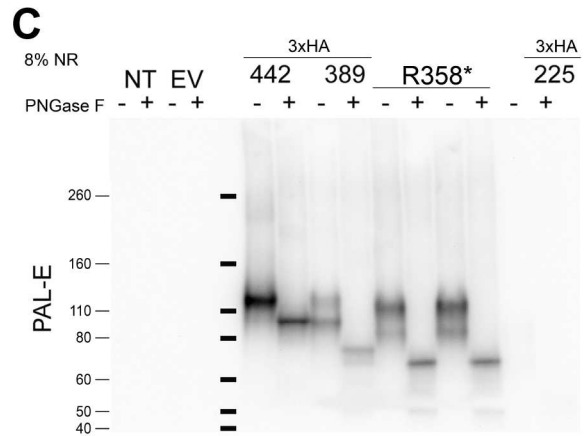
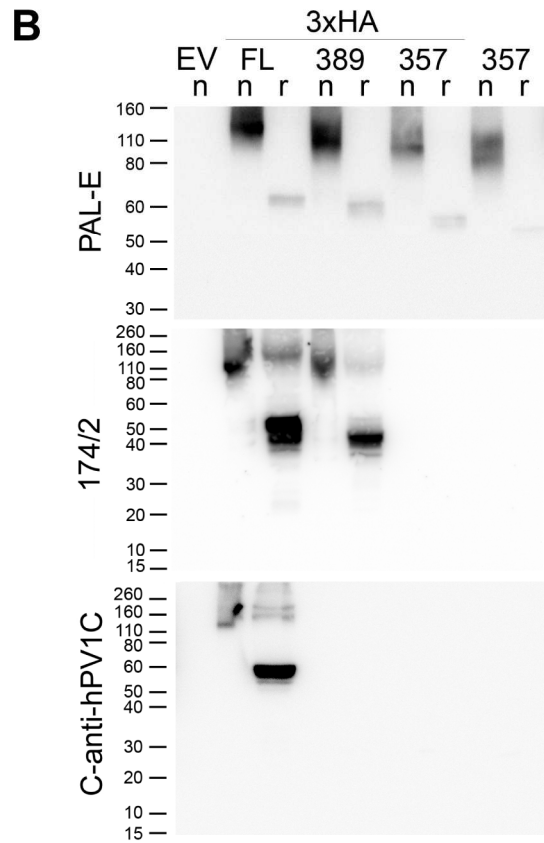
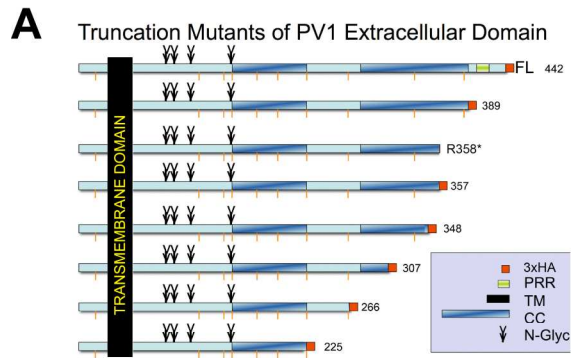
Figure 6: Proposed effect of PLVAP R358* mutation on endothelial fenestrae diaphragms.

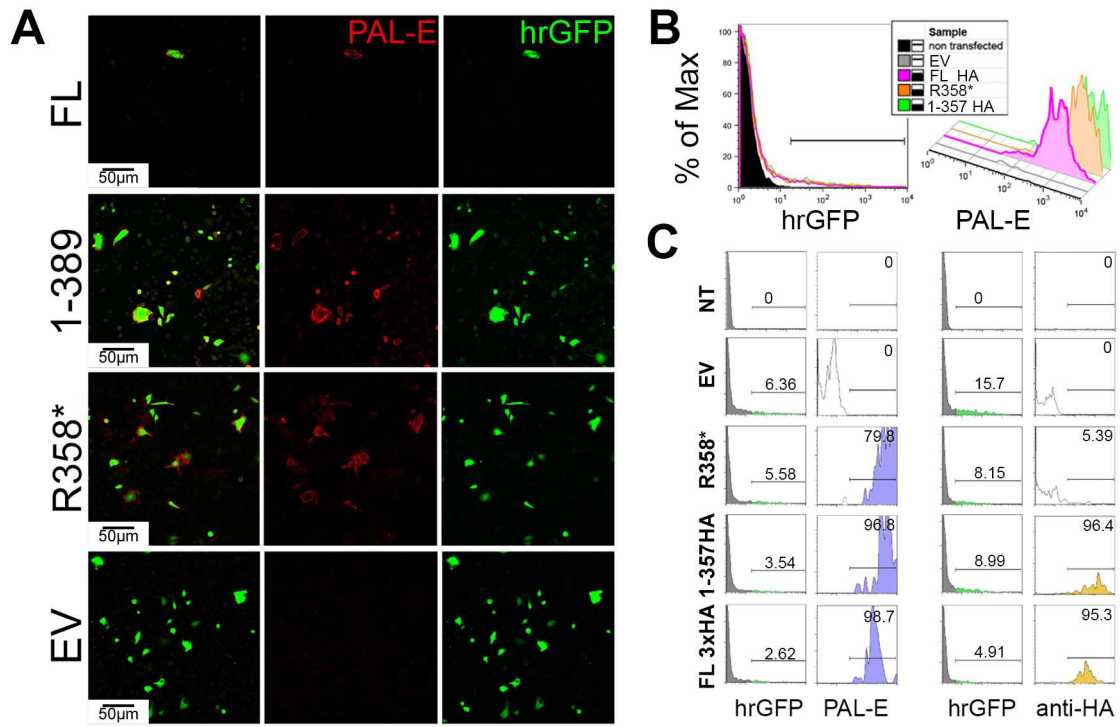
Expression of PLVAP leads to the formation of diaphragms in fenestrae (top). PLVAP R358* mutation results in the degradation of the vast majority of mRNA possibly via non-sense mediated decay (NMD) resulting in loss of PLVAP protein and failure in fenestrae diaphragm formation (bottom). Plasma proteins such as albumin (yellow) and immunoglobulins (blue) are subsequently lost due to absence of fenestrae.







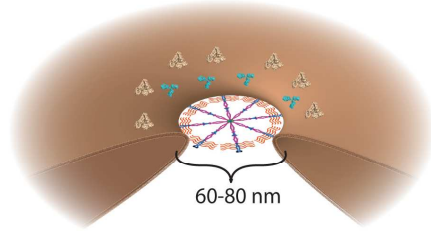




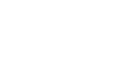
Normal PLVAP



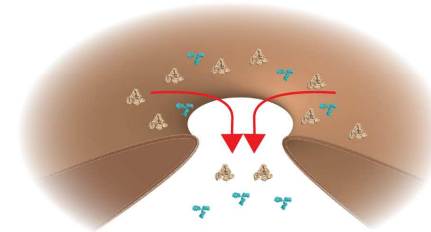
Dimerization



Mutated PLVAP



NMD



Supplemental Table 1: Clinical Laboratory Values

Red denotes initiation of Thyroxine therapy. Albumin above 10 g/l occurred when patient was on albumin infusion.

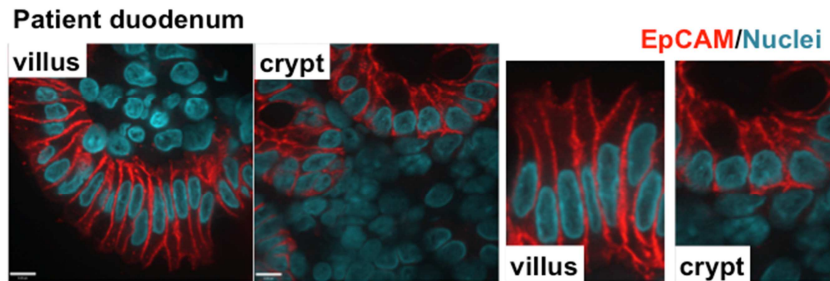
Age in Days	TSH (mIU/L)	Free T4 (pmol/L)	IgG (g/L)	IgA (g/L)	IgM (g/L)	IgE (g/L)	IgD (g/L)	Total Protein (g/L)	Albumin (g/L)	Conjugated Bilirubin (umol/L)	Unconjugated Bilirubin (umol/L)	ALT (U/L)	AST (U/L)	GGT (U/L)	Cholesterol (mmol/L)	HDL (mmol/L)	Triglycerides (mmol/L)
8	31.11	<5.1															
9									<10			33	16	90			
10									11								
11									10								
12	104.9	<5.1							11								
13									10								
14	108.9	<5.1							<10	0	0	28	13	71			
15								<20	<10								
16			<1.1	<0.1	0.3	<25	<26										
21	1.35											35	32	56			
22	3.71	12															
23								40	19	0	14						
29								41	19	0	1						
34	4.04							<20	<10	0	0	36	19				
35	5.78	11.9							10	0	0	42	33				
40									<10								
42	3.8	6							<10								
47			<1.1	<0.1	0.2	<25			<10								
50										0	0						
51	4.68	6.2															
55									<10								
58	11.51	9							<10	0	0	26	11	139			

Age in Days	TSH (mIU/L)	Free T4 (pmol/L)	IgG (g/L)	IgA (g/L)	IgM (g/L)	IgE (g/L)	IgD (g/L)	Total Protein (g/L)	Albumin (g/L)	Conjugated Bilirubin (umol/L)	Unconjugated Bilirubin (umol/L)	ALT (U/L)	AST (U/L)	GGT (U/L)	Cholesterol (mmol/L)	HDL (mmol/L)	Triglycerides (mmol/L)
64	4.06	8.3													3.22	0.34	6.86
71									<10				11		3.84	0.39	4.37
75										0	0						
82	1.03	12.2															
84									<10								
85												10					
89								24	11	0	0	29	14				
96								<20	<10	0	0	24	7				
103								20	<10	0	0	24	8				
110	0.85	9.4						<20	<10	0	0	27	12				
114									<10	0	0	23	11	223			
116									<10								
117								<20	<10	0	0	27	12				
119									11								
123									<10	0	0	27	29				
124	0.06	8.4	<1.1	0.1	0.6	<25		23	10	0	0	25	15				
128								<20	<10	0	0	21	17				
128								<20	<10	0	0	22	44				
133								<20	<10	0	0	20	82				
134	0.6	8.4						<20	<10								10.35
135								<20									
136	0.44	7.9							<10	0	0	42	26	290			

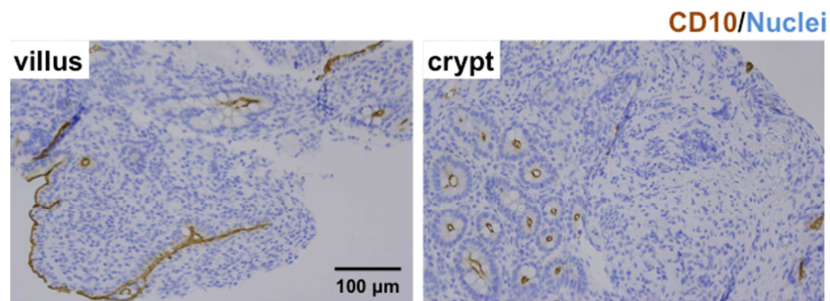
Category	Value
1	0.05
2	0.10
3	0.15
4	0.20
5	0.25
6	0.30
7	0.35
8	0.40
9	0.45
10	0.50
11	0.55
12	0.60
13	0.65
14	0.70
15	0.75
16	0.80
17	0.85
18	0.90
19	0.95
20	1.00
21	0.98
22	0.95
23	0.90
24	0.85
25	0.80
26	0.75
27	0.70
28	0.65
29	0.60
30	0.55
31	0.50
32	0.45
33	0.40
34	0.35
35	0.30
36	0.25
37	0.20
38	0.15
39	0.10
40	0.05

ACCEPTED MANUSCRIPT

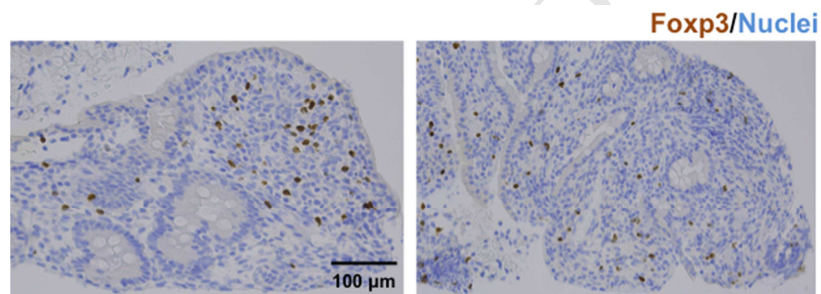
A



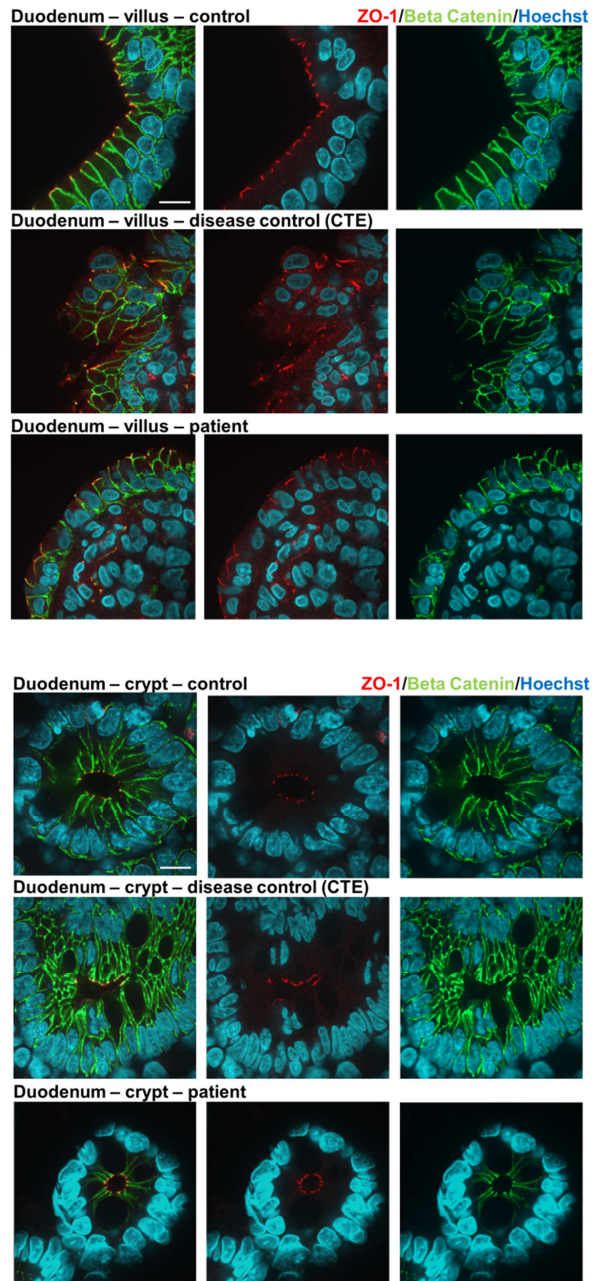
B



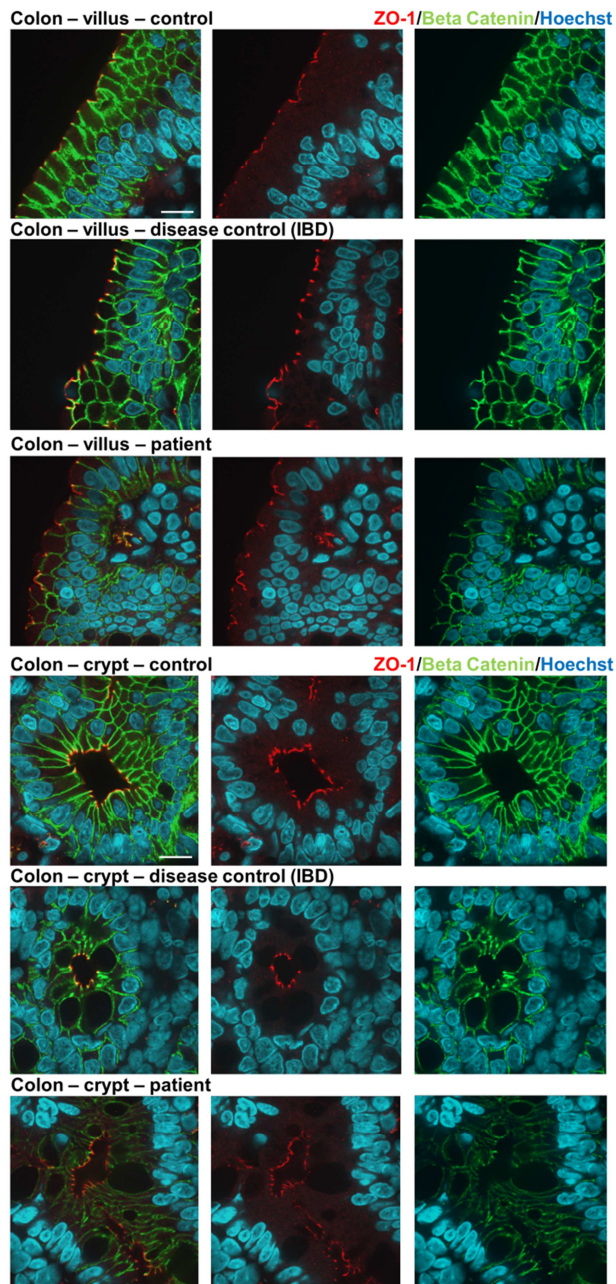
C



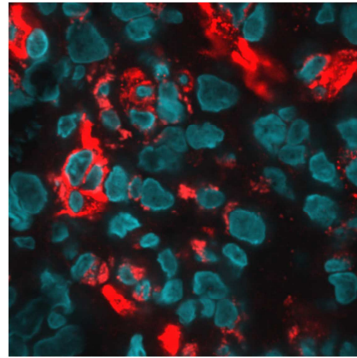
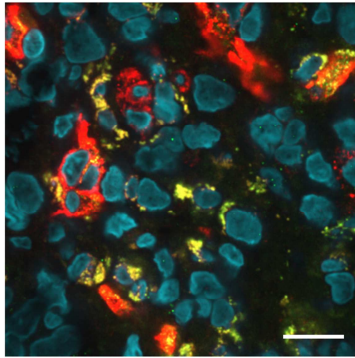
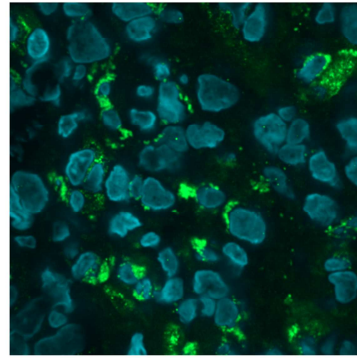
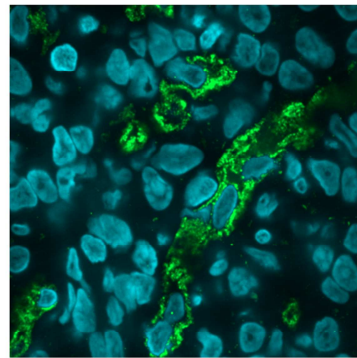
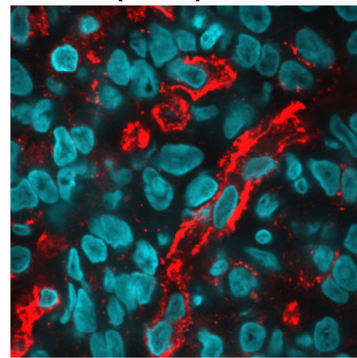
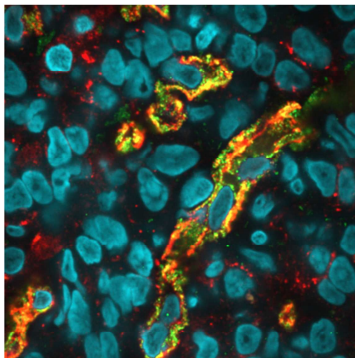
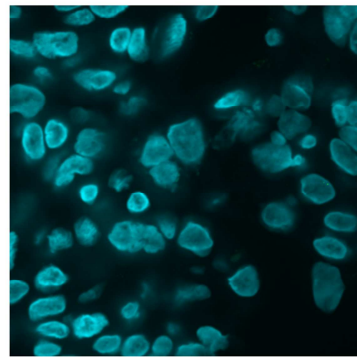
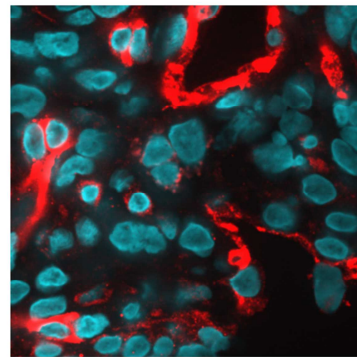
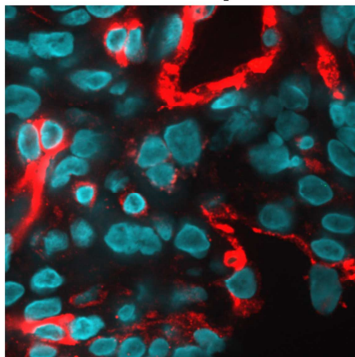
Supplemental Figure 1: Immunohistochemistry staining for epithelial cell adhesion molecule (EpCAM, panel A), CD10 (panel B) and Foxp3 (panel C) in duodenal biopsy samples from the patient. Normal expression and localization of EpCAM, CD10 and Foxp3 in the duodenum. Scale bars in panel A are 8 μ m; scale bars in panel B and C are 100 μ m.



Supplemental Figure 2A: Immunofluorescence analysis of tight junctions (ZO-1) and adherens junctions (Beta Catenin) in the duodenum of control, disease control and the patient. A congenital Tufting enteropathy (CTE) case presenting as protein losing enteropathy served as a proper disease control for the small intestine. ALEXA 568 red stains ZO-1, ALEXA 488 beta catenin and Hoechst nuclei in blue. ZO-1 localizes subapical and beta catenin basolateral in villus as well as crypt enterocytes of control, CTE and the patient. Scale bar is 10 μ m

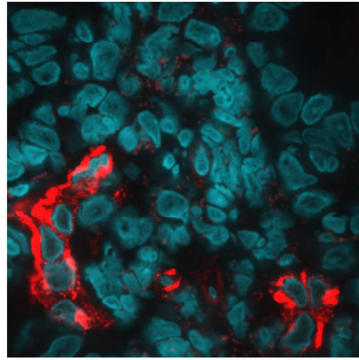
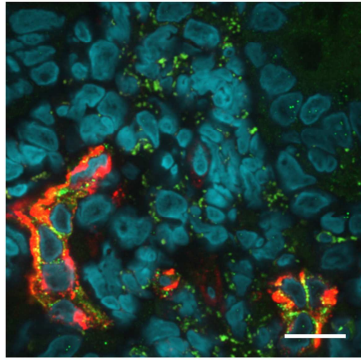


Supplemental Figure 2B: Immunofluorescence analysis of tight junctions (ZO-1) and adherens junctions (Beta Catenin) in the colon of control, disease control and the patient. A patient with inflammatory bowel disease (IBD) with active disease (inflamed areas in the colon) served as a disease control for the colon. ALEXA 568 red stains ZO-1, ALEXA 488 beta catenin and Hoechst nuclei in blue. ZO-1 localizes subapical and beta catenin basolateral in villus as well as crypt enterocytes of control, IBD case and the patient. Scale bar is 10 μ m

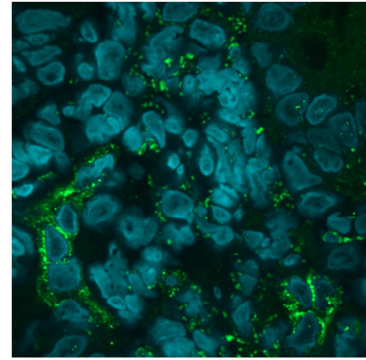
Duodenum – control**CD31/PLVAP/Hoechst****Duodenum – disease control (CTE)****Duodenum – patient**

Supplemental Figure 2C: Immunofluorescence analysis of vessels in the duodenum of control, disease control and the patient. A congenital Tufting enteropathy (CTE) case presenting as protein losing enteropathy served as a proper disease control for the small intestine. ALEXA 568 red stains CD31 (vessel marker), ALEXA 488 PLVAP and Hoechst nuclei in blue. CD31 marks the vessel walls and co-localizes with PLVAP in the control and CTE. In the patient the vessels are stained by CD31, but in the absence of PLVAP. Scale bar is 10 μ m

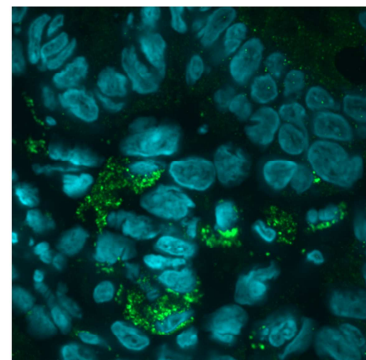
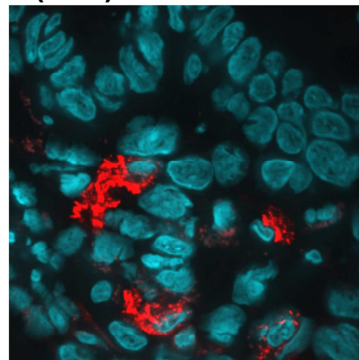
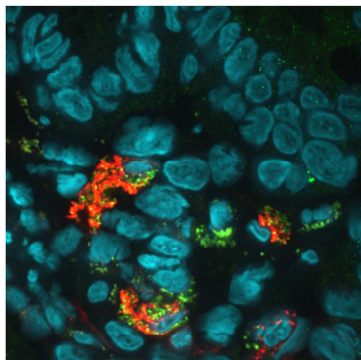
Colon – control



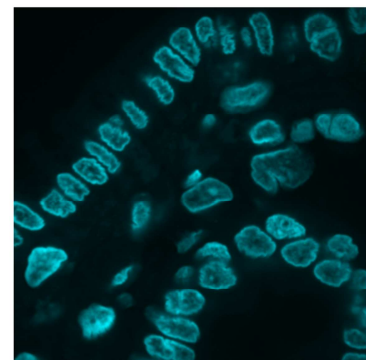
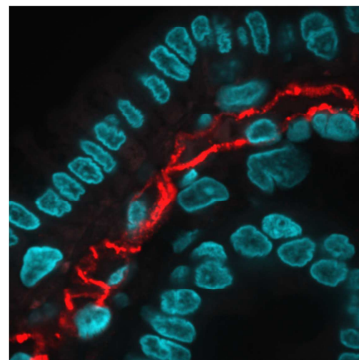
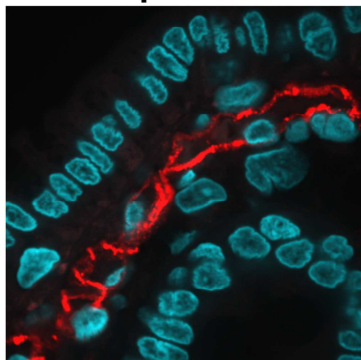
CD31/PLVAP/Hoechst



Colon – disease control (IBD)



Colon – patient



Supplemental Figure 2d: Immunofluorescence analysis of vessels in the colon of control, disease control and the patient. A patient with inflammatory bowel disease (IBD) with active disease (inflamed areas in the colon) served as a disease control for the colon. ALEXA 568 red stains CD31 (vessel marker), ALEXA 488 PLVAP and Hoechst nuclei in blue. CD31 marks the vessel walls and co-localizes with PLVAP in the control and IBD case. In the patient the vessels are stained by CD31, but in the absence of PLVAP. Scale bar is 10 μ m